Science of the Total Environment 715 (2020) 136906

Contents lists available at ScienceDirect

Science of the Total Environment

journal homepage: www.elsevier.com/locate/scitotenv

Lithium and strontium isotope dynamics in a carbonate island aquifer, Rottnest Island, Western Australia

A.N. Martin [a,b,c,d,*], K. Meredith [a,b], M.D. Norman [e], E. Bryan [a,b,c], A. Baker [a,c]

[a] Connected Waters Initiative Research Centre, UNSW Sydney, Sydney, NSW 2052, Australia
[b] Australian Nuclear Science and Technology Organisation, Lucas Heights, NSW 2234, Australia
[c] School of Biological, Earth and Environmental Sciences, UNSW Sydney, Sydney, NSW 2052, Australia
[d] Institut für Mineralogie, Leibniz Universität Hannover, Callinstraße 3, 30167 Hannover, Germany
[e] Research School of Earth Sciences, The Australian National University, Canberra, ACT 2601, Australia

HIGHLIGHTS

- Li isotopes were used for tracing groundwater sources in an island aquifer.
- Li and Sr mainly sourced from silicate weathering.
- Sodium mainly sourced from atmospheric input (rainfall and sea-spray aerosols).
- Increase in maximum δ^7Li in fresh groundwaters attributed to water-rock interactions.
- Decrease in minimum δ^7Li in deeper groundwaters attributed to silicate dissolution.

GRAPHICAL ABSTRACT

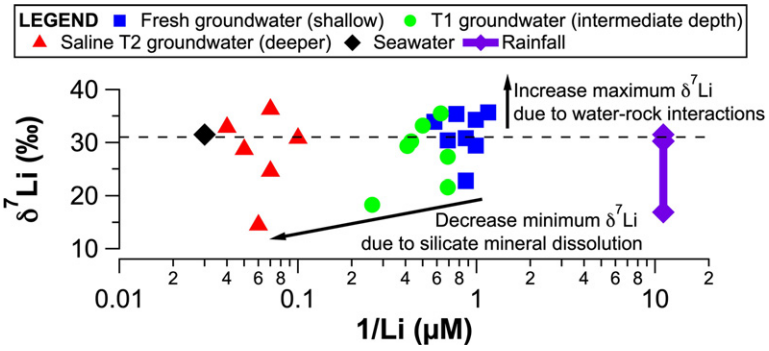

ARTICLE INFO

Article history:
Received 25 October 2019
Received in revised form 22 January 2020
Accepted 22 January 2020
Available online 23 January 2020

Editor: Mae Sexauer Gustin

Keywords:
Lithium isotopes
Groundwater
Karst
Carbonate
Aeolianite
Rottnest Island

ABSTRACT

Water-rock interactions in aquifer systems are a key control on water quality but remain poorly understood. Lithium (Li) isotopes are useful for understanding water-rock interactions, but there are few data available for groundwater aquifers. Here we present a Li isotope dataset for rainfall and groundwater samples from a carbonate island aquifer system: Rottnest Island, Western Australia. This dataset was complemented by strontium (Sr) isotope and major and trace element data for groundwaters, and leaching experiments on bedrock samples. The δ^7Li values and $^{87}Sr/^{86}Sr$ ratios of fresh groundwaters ranged from +23 to +36‰ and 0.709167 to 0.709198, respectively. Mass balance calculations indicated that silicate weathering supplied ~60 and 70% of dissolved Li and Sr in fresh groundwaters, respectively, with the remainder provided by atmospheric input, and carbonate weathering; for major cations, the majority of calcium and sodium (Na) are supplied by carbonate weathering and atmospheric input, respectively. The estimated low proportion of Sr produced by carbonate weathering was surprising in a carbonate aquifer, and the $^{87}Sr/^{86}Sr$ data indicated that the silicate Sr source had low Rb/Sr and $^{87}Sr/^{86}Sr$ ratios. There was an increase in the maximum δ^7Li values in fresh groundwaters (+36‰) relative to the maximum value in rainfall and seawater (ca. +31‰). As clay minerals are undersaturated in fresh groundwaters, this increase may be explained by Li isotope fractionation associated with ion-exchange reactions on clays and iron(oxy)hydroxides. In the more saline groundwaters, the minimum δ^7Li values decreased with depth to +14.5‰, suggesting increased silicate mineral dissolution in the deeper aquifer. These results reveal the importance of water-rock interactions in a coastal carbonate aquifer, and demonstrate the usefulness of Li

* Corresponding author at: Institut für Mineralogie, Leibniz Universität Hannover, Callinstrasse 3, 30167 Hannover, Germany.
E-mail address: a.martin@mineralogie.uni-hannover.de (A.N. Martin).

https://doi.org/10.1016/j.scitotenv.2020.136906

isotopes for tracing weathering reactions in an environmental setting where traditional weathering tracers, such as sodium and Sr isotopes, are less appropriate.

1. Introduction

It has long been recognised that water-rock reactions are the defining influence on groundwater chemistry (Garrels and Mackenzie, 1967; Goldenberg et al., 1984; Magaritz and Luzier, 1985). Stable isotope compositions of groundwaters can contribute to a better understanding of water-rock interactions by tracing their rate and extent in hydrological systems (DePaolo, 2011; Maher, 2011). Lithium (Li) isotopes (^{6}Li and ^{7}Li) are particularly useful for tracing water-rock interactions due to the preferential incorporation of ^{6}Li into secondary minerals during water-rock interactions (Huh et al., 1998; Pistiner and Henderson, 2003; Vigier et al., 2008). Therefore, dissolved δ^{7}Li values reflect the balance between silicate dissolution and secondary mineral formation, i.e., weathering congruency (Pogge von Strandmann and Henderson, 2015). In contrast to Li, the dissolved strontium (Sr) isotope ratio (^{87}Sr/^{86}Sr) provides information on the compositions of source rocks in the catchment or the aquifer lithologies (Elderfield, 1986). However, relative to silicate minerals, carbonates have faster dissolution rates and higher Sr contents so carbonate weathering tends to dominate the ^{87}Sr/^{86}Sr composition of dissolved loads (Blum et al., 1998).

The marine Li and Sr isotope records in carbonates are valuable archives of past changes in continental weathering over geological time. The average seawater δ^{7}Li value has increased by 9‰ from 60 Ma to the present, which has been inferred to reflect an increase in the rate of continental silicate weathering (Misra and Froelich, 2012). However, this interpretation is ambiguous due to assumptions and uncertainties regarding the global Li isotope budget. For instance, the change in δ^{7}Li value of seawater over the Cenozoic could be related to changes in soil production rates and Li storage in secondary minerals rather than changes in weathering and erosion rates (Vigier and Godderis, 2015). Despite submarine groundwater discharge (SGD) providing ~50% of the total dissolved solids (TDS) to the oceans (Zektser and Loaiciga, 1993), the global Li isotope budget is particularly under-constrained for groundwater systems (Pogge von Strandmann et al., 2014). Globally, the average dissolved δ^{7}Li values in shallow groundwater systems is ca. +15‰ (Meredith et al., 2013; Pogge von Strandmann et al., 2014; Bagard et al., 2015), which is lower than the average dissolved δ^{7}Li values in rivers (ca. +23‰, Huh et al., 1998). This may be due to prolonged water-rock interactions and the increased dissolution of ^{7}Li-depleted clay minerals within aquifer systems compared to surface waters (Bagard et al., 2015). Carbonate groundwater systems have received little attention with respect to Li isotopes. However, carbonate rocks cover 8–10% of Earth's ice-free dry surface (Dürr et al., 2005; Hartmann and Moosdorf, 2012), and are a ubiquitous feature of coastlines with 12% of the global submarine groundwater discharge (SGD) flux flowing through carbonate aquifers (Beck et al., 2013). Many coastal carbonate rocks are young (typically Late Quaternary) carbonate aeolianites (Brooke, 2001), which undergo extensive carbonate recrystallisation reactions (Appelo and Postma, 2005; Bryan et al., 2017) and can have average silicate mineral contents up to 42 wt% (Lipar and Webb, 2014). Carbonate aeolianites also frequently contain paleosol units with abundant clays and iron oxides that may preferentially adsorb ^{6}Li and produce high δ^{7}Li groundwaters. Calcite precipitation in carbonate groundwater systems may also fractionate Li isotopes as ^{6}Li is preferentially incorporated during calcite precipitation with a fractionation factor of ~8.5‰ (Marriott et al., 2004), which is similar to the difference between dripwaters and speleothem calcite (3.6–5.2‰) measured in two Israeli caves (Pogge von Strandmann et al., 2017). Another major assumption regarding the global Li isotope weathering cycle is that the δ^{7}Li continental weathering signal of meteoric waters is not modified during seawater mixing (Misra and Froelich, 2012). In fact, estuarine processes may remove 15–25% of dissolved Li supplied by rivers globally (Pogge von Strandmann et al., 2008; Murphy et al., 2014). Therefore, the cycling of Li isotopes in coastal carbonate aquifers and during seawater mixing are key areas for refining the global Li budget.

Here we present the Li and Sr isotope ratios of groundwater samples from a coastal carbonate aquifer on Rottnest Island, Western Australia. Existing conventional stable isotope data (^{2}H, ^{13}C, and ^{18}O), tritium (^{3}H), radiocarbon (^{14}C) measurements, major/trace cations, and major anions further assist the interpretation of stable isotope systematics and fractionation processes from source (rainfall) to sink (seawater). We report Li and Sr data for 1) seasonal rainfall and shallow, fresh groundwater samples that have not undergone seawater mixing and represent rainfall recharge into the carbonate aquifer, and 2) deeper, more saline groundwaters that have undergone seawater mixing (Bryan et al., 2017; Bryan et al., 2016). We first determine the proportions of Li and Sr derived from the various sources using a simple mass balance approach. We then discuss the evolution of groundwater Li and Sr isotope ratios in fresh, shallow groundwaters and then in deeper, more saline groundwaters to assess the extent of water-rock interactions occurring in the various aquifer compartments. These data provide the first Li isotope measurements in a carbonate island aquifer system, and in rainfall samples from the Southern Hemisphere.

2. Study area

2.1. Geomorphology and climate

Rottnest Island (RI) is a small (~19 km^{2}) carbonate aeolianite island located 18 km from Perth, Western Australia with a maximum elevation of ~45 m Australian Height Datum (AHD) (Fig. 1). It is part of the world's longest (~1000 km) carbonate aeolianite deposit, extending from Albany to Shark Bay (25–35°S) (Brooke, 2001). It is an A-Class reserve under the Land Administration Act 1997 that limits all activities that may disturb its environment. Since it was settled by Europeans in the 1830s CE, it has been used as a prison, military training area, agricultural area, and is now primarily a tourist destination. European settlement reduced the native vegetation cover to 23% by 1941 CE, and 5% by 1997 CE (Playford, 1997). Revegetation has recently commenced on the island, but the area above the freshwater lens remains cleared to increase groundwater recharge. Undulating sand dune hills characterise most of the island, with an absence of water courses due to the highly permeable carbonate lithology. The island is similar to other carbonate aeolianite islands, such as The Bahamas, which are characterised by dune shaped topography, large amplitude, high-angle cross-bedding, paleosols, and fossiliferous marine units (Vacher and Quinn, 1997).

Rottnest Island has a Mediterranean-type climate characterised by hot and dry summers, with mild and wet winters (Bryan et al., 2016). The long-term average rainfall is 691 mm/a (1880–2015 CE) and annual reference evapotranspiration (ET) is 1694 mm/a. On RI, there has been low average mean annual rainfall since the 1960s CE due to a regional drying trend (Bryan et al., 2016). There are several permanent hypersaline lakes on RI at ~0 m AHD that cover ~10% of the island (Playford et al., 1977), and some lower salinity inter-dunal swamps (Gouramanis et al., 2012).

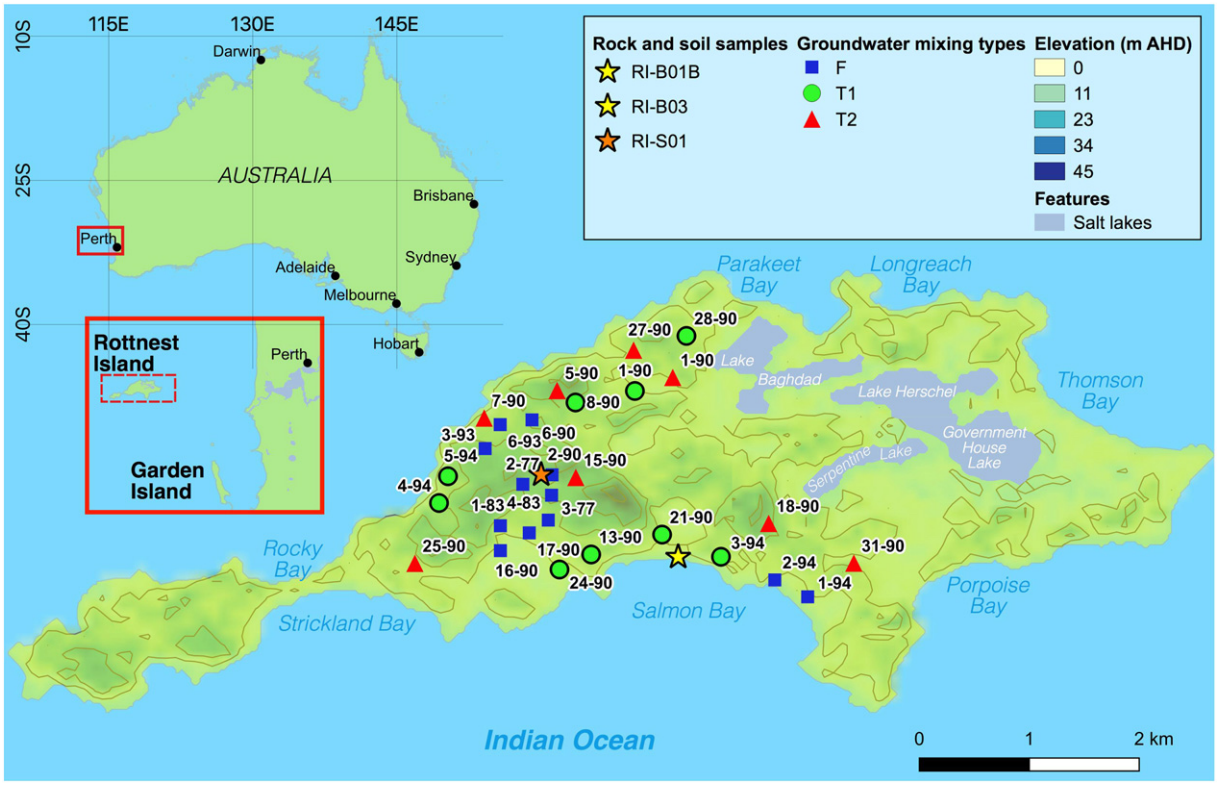

Fig. 1. Digital Elevation Model of Rottnest Island, Australia showing groundwater, rock and soil sampling locations and IDs. Groundwater mixing types are defined according to Bryan et al. (2017) (see Table A.1).

2.2. Geology and hydrology

Rottnest Island predominantly comprises Tamala Limestone that is a Pleistocene to mid-Holocene carbonate aeolianite with a thickness of ~115 m (Playford et al., 1977). Tamala Limestone is typical of Late Quaternary coastal aeolianites that are widely distributed globally (Brooke, 2001). It is a strongly-lithified to friable rock that is creamy-white to yellow, or light-grey in colour. There are varying proportions of silicate sand grains (predominantly quartz), fine- to medium-grained shell fragments, and fine- to coarse-sand-sized carbonate bioclasts (Playford, 1997). Tamala Limestone units on RI include dune, paleosol, and shallow marine units. Paleosol units generally contain higher proportions of quartz and clays than surrounding calcarenites, representing periods of reduced dune development and soil formation (Playford et al., 1977; Lipar and Webb, 2014). Tamala Limestone lies unconformably upon Cretaceous fluvial sand beds (Playford et al., 1976). The proportion of quartz and feldspars in Tamala Limestone from RI is highly variable and ranges from 4 to 79 wt% with a mean of 42 wt% (Lipar and Webb, 2014).

A freshwater lens is located within the upper Tamala Limestone that extends from ca. 0 to 10 m below present sea level (bpsl) above a transition zone that extends from ca. 10 to 50 m bpsl (Playford, 1997). The volume of the freshwater lens has contracted significantly since the late 1970s CE due to a decline in precipitation since the mid-1960s CE, resulting in seawater intrusion (Bryan et al., 2016). Groundwater recharge at present mainly occurs during winter rainfall and episodic rainfall events (Bryan et al., 2020). Sea level high stands (~2 m higher than present) occurred at ~7 and 4 ka (Gouramanis et al., 2012) that likely caused seawater intrusion events into the aquifer. A sulfate deficit in the deeper, more saline T1 and T2 groundwaters indicates that anoxic conditions may be present in the deeper aquifer (Bryan et al., 2016). Moreover, the mixing of fresh groundwaters and seawater in the deeper aquifer promotes additional geochemical reactions, such as sulfate reduction, mixing corrosion, and ion exchange (Bryan et al., 2017).

3. Field procedures

Twenty-nine groundwater samples were collected from production and monitoring wells during two field campaigns in September 2014 and March 2015 (Fig. 1). Monitoring well samples were collected using a plastic submersible centrifugal pump (Supernova 120), while production well samples were collected using permanently installed production pumps. Samples were collected at, or just above the well screens, which are located at the bottom of each well and measure a maximum of 1.5 m in length. One seawater sample was also collected using a peristaltic pump (Masterflex E/S portable sampler). Temperature, pH, electrical conductivity and dissolved oxygen were measured in the field using a YSI 556 Multiparameter Instrument. After standing water levels were measured, the monitoring wells were purged of three well volumes and until stabilisation of in-field parameters. Production wells were purged until stabilisation of in-field parameters before groundwater samples were collected. Total alkalinity concentrations were determined by a double end-point titration method using a HACH digital titrator at a dedicated field laboratory at the end of each day.

Composite rainfall samples were obtained on a weekly basis from May 2014 to March 2015 in a rainfall collector designed to minimise evaporation for isotopic analysis. Samples for major ions were collected in 30 mL HDPE bottles, and sealed with tape after collection to limit atmospheric exchange. All samples were filtered and acidified with 65% Suprapur® HNO_3 in the laboratory.

Tamala Limestone rock samples were collected during a field trip to RI in March 2017. For rock samples, weathered material was removed using a geological hammer, and only visibly-unweathered material was sampled. A dull brown-red paleosol unit (RI-B01B) and a cream-white aeolianite unit (RI-B03) were sampled from an outcrop at Salmon Bay (32°00′46″S 115°30′33″E). In addition, a dull brown soil sample (RI-S01) was collected from an actively-forming dune on an exposed ridge in the unvegetated centre of the island above the freshwater lens (32°00′19″S 115°29′48″E) (Fig. 1).

4. Analytical techniques

4.1. Major cation and anion concentrations

Rock end-members were dissolved by leaching and strong-acid dissolution at the Australian Nuclear Science and Technology Organisation (ANSTO). Approximately 1 g of sample was weighed into centrifuge tubes and the acid-soluble fraction was first removed by adding 40 mL of 0.5 M hydrochloric acid (HCl) and agitating for 1 h at room temperature. The aqueous phase was then removed by centrifugation and retained for analyses. To dissolve the remaining solid residue, 0.5 mL of conc. nitric acid (HNO_3) and 2 mL of conc. hydrofluoric acid (HF) were added, and heated at 120 °C overnight. These solutions were then evaporated at 100 °C until the solid residue reached incipient dryness. To ensure complete dissolution of the solid phase, 0.5 mL of conc. HNO_3 and 1.5 mL of conc. HCl (aqua regia) were added and heated overnight at 120 °C. The solutions were then evaporated at 100 °C until the solid residue reached incipient dryness. Finally, 0.1 mL of conc. HNO_3 was added to the solid residues and evaporated at 100 °C until the solid residue reached incipient dryness. The solid residue was then re-dissolved in 2% v/v HNO_3 for ICP-MS analysis.

The chemical composition of water samples and rock end-members were analysed at the ANSTO by ion chromatography and inductively coupled plasma-atomic emission spectroscopy for anions and cations respectively. Cations and anions were assessed for accuracy by evaluating the charge balance error, with 80% of the samples falling within ±5% and all samples falling within ±6.2%.

4.2. Lithium isotopes

Lithium isotope column chromatography procedures were conducted in clean laboratories at ANSTO. Acids used were high-purity SEASTAR™ IQ grade HCl and HNO_3, which were further purified by sub-boiling using Savillex® PFA distillation apparatus. All dilutions were carried using >18.2 MΩ.cm at 25 °C Milli-Q® water. Acid concentrations were determined by titration. Column chromatography was conducted using 8 mL Biorad AG 50W-X8 (100–200) cation exchange resin packed in Savillex® 6.4 mm × 25 cm microcolumns based on the one-step procedure from Van Hoecke et al. (2015). Column calibration experiments were conducted to ensure 100% Li yield, which was found to be the 15–37.5 mL 0.5 M HCl fraction (Fig. A.1; Table A.1). Prior to sample loading, columns were cleaned with three column volumes of 6 M HCl to prevent Na contamination from the resin (Van Hoecke et al., 2015), and then conditioned with three column volumes of 0.5 M HCl. A volume of sample containing 50 ng of Li was loaded and eluted using 0.5 M HCl. Columns cuts for each sample were collected in Savillex® PFA vials and evaporated to incipient dryness at 80 °C. The residues were then re-dissolved in 2 mL of 2% (v/v) HNO_3 to yield samples containing 25 ppb Li for isotopic analysis. Isotopic standards were processed through the column chemistry to reproduce conditions for the samples. Column cuts were retained before and after the Li fraction to verify a 100% Li yield for each sample.

Lithium isotope ratios were measured by multi-collector inductively coupled plasma mass spectrometer (MC ICP-MS) using a Thermo Scientific™ Neptune Plus™ in low-resolution mode at the Research School of Earth Sciences (RSES), Australian National University (ANU). The instrument tuning settings were adjusted prior to each analytical session to achieve the optimum balance between high signal sensitivity and stability, and the instrument was operated for a few hours prior to sample measurements. The sensitivity for ^7Li was ~8 V/ppb measured in faraday cups equipped with $10^{11}\Omega$ resistors. Isotopic ratios were corrected using an external standard-sample-standard bracketing approach (Albarède and Beard, 2004) and samples were screened prior to analysis to ensure that the signal intensities of samples and standard were within ~10% of each other. The isotopic reference material used for bracketing was a 50 ppb solution of the synthetic lithium carbonate powder IRMM-016 (Qi et al., 1997). For rainfall samples with low Li concentrations, Li concentrations were estimated from the MC-ICPMS signal intensity using the original volume of the sample solution, the final analysed volume, the known concentration of the IRMM-016 solution, and verifying a 100% yield during column chromatography. Corrected Li isotope ratios of samples and standards are presented as δ^7Li (in ‰) as variations relative to the L-SVEC standard (where $\delta^7Li = [(^7Li / {}^6Li)_{sample} / (^7Li / {}^6Li)_{L\text{-}SVEC} - 1] \times 1000$. The average δ^7Li value for IRMM-016 was +0.26 ± 0.10‰ (2SD, n = 5), which is within uncertainty of the long-term average of reported values +0.20 ± 0.20‰ (2SD, n = 52) (Millot et al., 2004). A Southern Ocean seawater sample was analysed as an unknown and had a δ^7Li value of +30.8 ± 0.1‰ (2SE, n = 1), which is also within uncertainty of the global average seawater value of +31.0 ± 0.5‰ (Misra and Froelich, 2012). The Li signal intensities for total procedural blank samples and retained cuts of the non-Li fractions from column chromatography could not be distinguished from the background signal (ca. 2 mV for ^7Li) during MC-ICP-MS analyses, which were measured in 2% (v/v) HNO_3.

4.3. Strontium isotopes

$^{87}Sr/^{86}Sr$ isotope ratios were measured at RSES, ANU. Samples were measured by thermal ionisation MS following purification of the Sr by ion-specific resin chromatography (Eichrom Sr-spec). Analyses were normalised to $^{86}Sr/^{88}Sr = 0.1194$ to correct for mass fractionation during analysis. Replicate measurements of NBS 987 run with these samples yielded an average $^{86}Sr/^{88}Sr$ value of 0.710253 ± 0.000003 (2SE, n = 7).

4.4. XRD measurements

Samples were measured using a PANalytical Powder X-ray diffractometer, Empyrean with Co as anode at 45 kV and 40 mA X-ray generation condition using following optics: Incident Beam Optics: BBHD optics with 0.5° divergence slit and 1° anti-scatter slit, 10 mm beam mask and 0.04 rad Soller slit. PANalytical HighScore Plus software was used for data processing and ICDD database was used to search candidate pattern of possible crystalline phases in the samples. Rietveld fit using the same HighScore Plus software was performed on the raw data in order to estimate the percentage composition of mineral phases in each sample.

5. Results

5.1. Rainfall

The Li concentrations of RI rainfall samples were estimated to range from 0.05 to 0.12 μM, with an average of 0.09 μM (Table 1). The austral autumn and summer samples exhibited higher Li concentrations (0.05 to 0.07 μM) than the winter and spring events (0.10 to 0.12 μM). A higher average Li rainfall concentration is reported in other oceanic island settings (0.72 μM, Table 1), corresponding to rainfall measured on the volcanic islands of Hawai'i, The Azores and Guadeloupe. The δ^7Li values of RI rainfall samples ranged from +16.9 to +31.5‰ (Table 1). The average of these values (+27.2 ± 6.9‰, 1SD) is similar to that of seawater (ca. +31‰), ice sampled from a glacier in Iceland (Pogge von Strandmann et al., 2006) and rainfall from the Azores archipelago (Pogge von Strandmann et al., 2010). The lowest rainfall δ^7Li value on RI (+16.9‰) was measured during the austral autumn and may reflect a higher proportion of continental aerosols, such as observed previously in rainfall samples from France (Millot et al., 2010) and Hawai'i (Pistiner and Henderson, 2003).

The Sr concentrations of RI rainfall samples from the austral spring and summer (0.59 and 1.22 μM, respectively) were higher than those sampled during autumn and winter (0.33 to 0.34 μM, respectively), with an average of 0.62 μM (Table 1). The Sr concentrations in RI rainfall

Table 1
Li data for filtered rainfall samples from Rottnest Island, including global rainfall and ice[a] samples from other sources.

Sample ID	Li (μM)	Sr (μM)	δ^7Li (‰)	Source
Autumn (MAM)	0.10	0.33	+16.9	This study
Winter (JJA)	0.07	0.34	+31.5	This study
Spring (SON)	0.05	0.59	+30.3	This study
Summer (DJF)	0.12	1.22	+30.2	This study
Rottnest Island – average	0.09	n/a	+27.2 ± 6.9	This study
Hawaii	0.01	n/a	+14.3	Pistiner and Henderson (2003)
Iceland[a]	2.12	n/a	+33.3	Pogge von Strandmann et al. (2006)
Azores Archipelago	0.02	n/a	+32.8	Pogge von Strandmann et al. (2010)
Guadelope, Lesser Antilles	<0.01 to 0.01	n/a	+11.2 to +26.4	Clergue et al. (2015)
Brest, France 2003–2004	0.06	n/a	+22.5 ± 4.3	Millot et al. (2010)
Dax, France 2003–2004	0.07	n/a	+22.8 ± 4.3	Millot et al. (2010)
Orleans, France 2003–2004	0.05	n/a	+16.1 ± 4.8	Millot et al. (2010)
Clermont-Ferrand 1994–1995	0.06	n/a	+26.2 ± 29.7	Millot et al. (2010)

are all at least two-fold higher than that of a coastal rainfall sample from southern Australia (0.14 μM) (Raiber et al., 2009). The summer rainfall sample exhibited the highest Li and Sr concentrations but for rainfall samples there was no correlation between Li and Sr concentrations, or Li and δ^7Li values (Fig. A.2).

5.2. Groundwaters

Groundwater Li concentrations ranged from 0.58 to 25.79 μM with an average of 5.71 μM and a local seawater Li concentration of 33.28 μM (Table 2). Groundwaters at RI are grouped into three types according to their elevation and hydrogeochemical parameters: fresh (F), Transition 1 (T1), and Transition 2 (T2) (Bryan et al., 2017) (see Table A.2 for definitions). In fresh groundwaters with a seawater abundance of <1% (Bryan et al., 2016), the average Li concentration in groundwaters in the karst lithology at RI is higher than that of cave dripwaters (Pogge von Strandmann et al., 2017), and the alluvial aquifer in the Bay of Bengal, India (Bagard et al., 2015), but lower than some other alluvial aquifers (Négrel et al., 2012; Meredith et al., 2013; Pogge von Strandmann et al., 2014), a sedimentary aquifer (Millot et al., 2011), a volcanic lithology (Liu et al., 2015). Groundwater Sr concentrations ranged from 10.0 to 260.0 μM with a local seawater concentration of 70.0 μM (Table 2). The average Sr concentration in fresh groundwaters was 27.5 μM, which is an order of magnitude higher than the global average groundwater value of 2.9 μM (Beck et al., 2013), similar to groundwaters draining other carbonate lithologies (Banner et al., 1994; Martin and Moore, 2008; Beck et al., 2013).

Lithium concentrations in groundwaters generally followed a linear mixing line between the freshest groundwater (RI_2-94) and local seawater (Fig. 2A), similar to Mg, Na and K concentrations (Fig. 2D, E, and F). In contrast, Sr, Ca and Si concentrations did not follow clear seawater mixing lines (Fig. 2B, C and G). The slight enrichment in Li, Ca and Mg concentrations in fresh groundwaters relative to conservative mixing with seawater may be explained by the dissolution of minerals in the aquifer releasing these cations. The extent of seawater mixing is indicated by Cl concentrations and this generally increases with increasing

Table 2
Groundwater sample parameters, sample concentrations and isotopic ratios.

ID	Mixing type	Sampling date	Screen elevation	Ca	Mg	Na	Cl	Li[a]	Si[a]	Sr[a]	δ^7Li	$^{87}Sr/^{86}Sr$
			m AHD[2]	mM	mM	mM	mM	μM	μM	μM	‰	–
RI_2-77	F	9/29/14	−0.11	1.0	1.7	4.3	4.6	1.01	81.9	30.0	29.4	0.7091717
RI_3-77	F	9/29/14	−0.01	1.3	2.1	4.5	5.1	0.86	89.0	30.0	35.7	0.7091879
RI_1-83	F	9/28/14	0.09	1.4	1.8	4.9	6.1	1.44	124.6	40.0	30.4	0.7091674
RI_4-83	F	9/30/14	−0.11	1.1	2.0	3.8	4.4	1.01	113.9	40.0	34.3	0.7091673
RI_2-90	F	9/29/14	−0.50	1.0	1.5	3.6	4.2	0.72	74.8	20.0	NA	0.7091843
RI_6-90	F	9/29/14	−0.64	1.5	1.6	5.4	6.8	1.15	135.3	20.0	30.8	0.7091981
RI_16-90	F	9/28/14	−0.28	1.6	1.9	4.7	5.9	1.73	138.9	40.0	33.9	0.7091815
RI_17-90	F	9/30/14	0.06	1.2	2.0	5.1	5.9	1.30	121.1	40.0	35.4	0.7091795
RI_3-93	F	9/29/14	−0.27	1.2	2.0	6.1	7.5	1.30	117.5	30.0	35.4	0.7091884
RI_6-93	F	9/29/14	−0.22	1.2	1.7	4.3	5.5	1.15	131.7	20.0	22.8	0.7091924
RI_1-94	F	9/28/14	−0.53	1.5	1.3	3.7	4.6	1.30	85.5	10.0	NA	NA
RI_2-94	F	9/28/14	−1.00	1.5	0.7	2.3	2.7	0.58	128.2	10.0	NA	NA
RI_1-90	T1	9/29/14	−0.90	1.9	3.8	26.4	35.1	2.45	128.2	50.0	29.4	0.7091802
RI_8-90	T1	9/29/14	−0.59	1.5	2.6	8.9	9.2	1.58	192.3	30.0	35.5	0.7091861
RI_7-90	T1	3/12/15	−7.06	6.8	31.5	275.4	320.9	NA	0.0	60.0	NA	0.7091981
RI_13-90	T1	3/11/15	−3.55	2.5	7.6	59.3	74.1	0.00	0.0	80.0	33.0	NA
RI_21-90	T1	9/26/14	−4.04	2.9	5.6	38.5	46.4	3.89	117.5	30.0	18.3	0.709191
RI_24-90	T1	9/26/14	−3.47	1.5	2.6	9.0	11.9	2.02	131.7	40.0	33.2	NA
RI_28-90	T1	9/26/14	−1.52	2.2	2.6	20.6	27.4	2.31	113.9	40.0	30.2	NA
RI_3-94	T1	9/27/14	−0.72	1.8	2.0	10.8	13.7	1.44	78.3	10.0	21.6	0.709258
RI_4-94	T1	9/27/14	−1.83	1.4	2.8	7.3	8.9	1.44	174.5	50.0	NA	NA
RI_5-94	T1	9/27/14	−1.87	1.3	2.6	7.5	8.9	1.44	128.2	60.0	27.3	0.708144
RI_5-90	T2	9/27/14	−6.90	3.9	10.5	93.3	97.0	10.23	195.8	130.0	30.8	NA
RI_11-90	T2	9/26/14	−6.19	9.6	41.8	383.7	473.2	25.79	81.9	130.0	32.9	0.709251
RI_15-90	T2	9/26/14	−14.92	7.1	32.9	282.8	381.0	17.58	106.8	260.0	14.5	0.709198
RI_18-90	T2	9/27/14	−11.16	7.4	37.9	312.0	409.1	22.19	64.1	60.0	NA	NA
RI_25-90	T2	9/27/14	NA	4.9	22.2	187.9	225.0	13.40	99.7	100.0	36.3	0.709196
RI_27-90	T2	9/26/14	−4.98	7.0	32.3	288.5	308.9	20.60	113.9	100.0	28.7	0.709186
RI_31-90	T2	9/28/14	−9.20	7.7	25.6	217.1	244.2	14.41	85.5	60.0	24.6	NA
SW	–	3/12/15	0.00	10.1	54.2	480.7	560.6	33.28	3.6	70.0	33.0	NA

[a] 1SD uncertainty is ±6.2%.

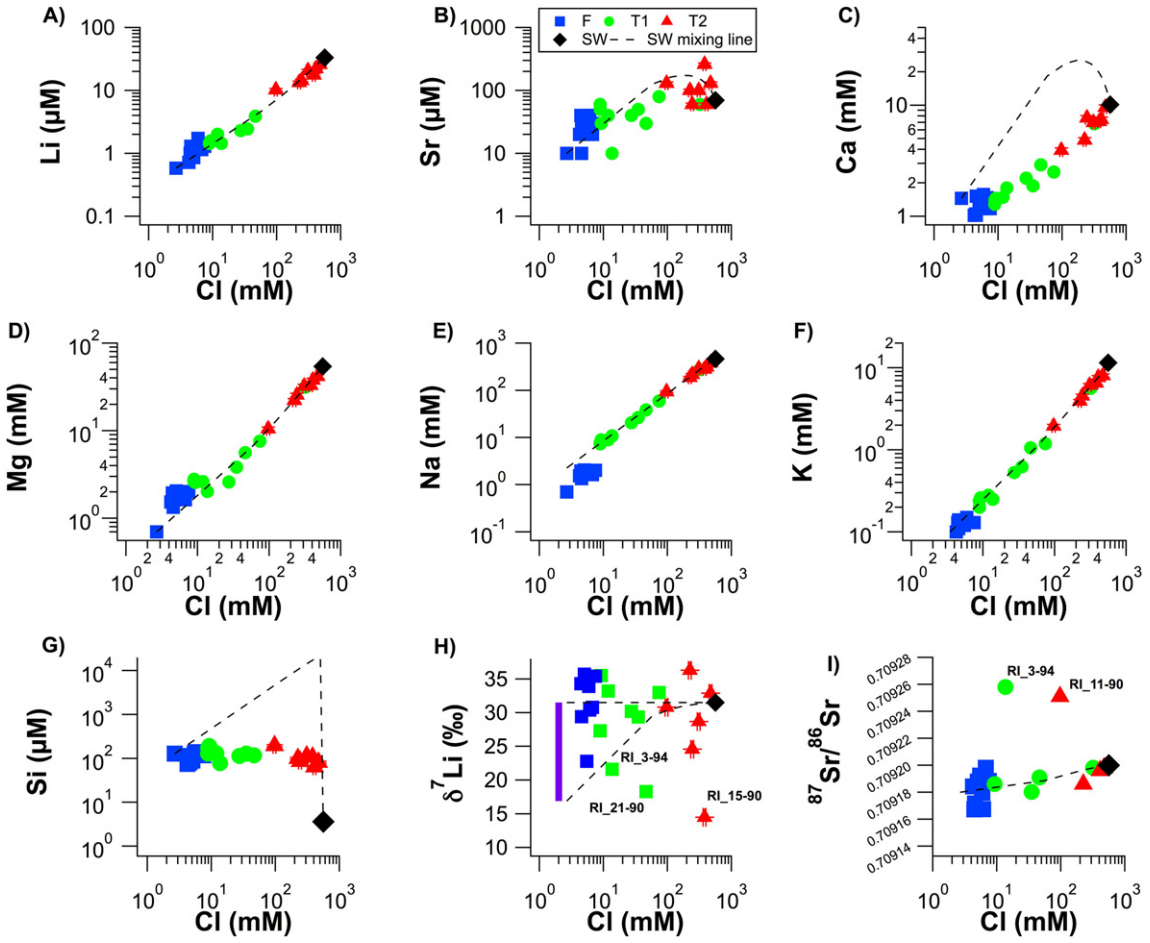

Fig. 2. A) Li, B) Sr, C) Ca, D) Mg, E) Na, F) K, G) Si concentrations, and H) Li isotope ratios and I) Sr isotope ratios as a function of Cl concentrations in groundwaters. Dashed black lines in concentration-concentration plots show predicted mixing lines between seawater (SW) and the freshest groundwater (RI_2-94). The two dashed black lines in H) show mixing between the two end-member rainfall Li isotope compositions (+16.9 and +31.5‰; Table 1) and seawater. The dashed line in I) shows the mixing line between the average $^{87}Sr/^{86}Sr$ ratio of fresh groundwaters (0.70918) and an assumed seawater composition of 0.70920 (Elderfield, 1986).

depth in the aquifer (Fig. 3A). Due to the higher Li concentration in seawater, there is also a general increase in Li concentration with depth. However, there is no relationship with depth when only each group (fresh, T1 or T2) of groundwaters (Fig. 3B).

The δ^7Li values of groundwaters ranged from +14.5‰ to +36.3‰ with an average δ^7Li value of +29.8‰ (1SD = 5.9, n = 23, Table 2). There was no correlation between δ^7Li values and inverse Li concentrations (1/[Li]; Fig. 4), which is inconsistent with simple binary mixing and indicates that multiple sources and/processes contributed to the Li distributions in these waters. The average groundwater δ^7Li value at RI is generally higher than the average values measured in other groundwater systems, which range from approximately +8 to +22‰ (Millot et al., 2011; Négrel et al., 2012; Meredith et al., 2013; Bagard et al., 2015; Pogge von Strandmann et al., 2017). Higher δ^7Li values (>+31‰) are reported in alkaline lake systems, e.g., the Mono Basin, U.S. (Tomascak et al., 2003). The $^{87}Sr/^{86}Sr$ ratios ranged from 0.709167 to 0.709258 with an average value of 0.709192 (n = 19) (Table 2), excluding well RI_5-94 that had an anomalously low $^{87}Sr/^{86}Sr$ ratio of 0.708144. There was no correlation between $^{87}Sr/^{86}Sr$ ratios and inverse Sr concentrations (1/[Sr]; Fig. 4B), which, similar to Li, indicates that the

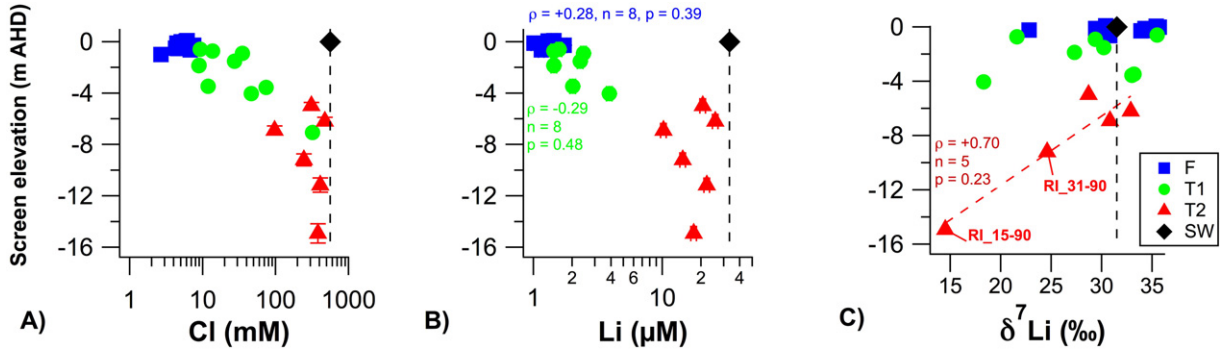

Fig. 3. Screen elevation as a function of groundwater A) Cl and B) Li concentrations and C) δ^7Li values where ρ: Spearman's rank correlation coefficient.

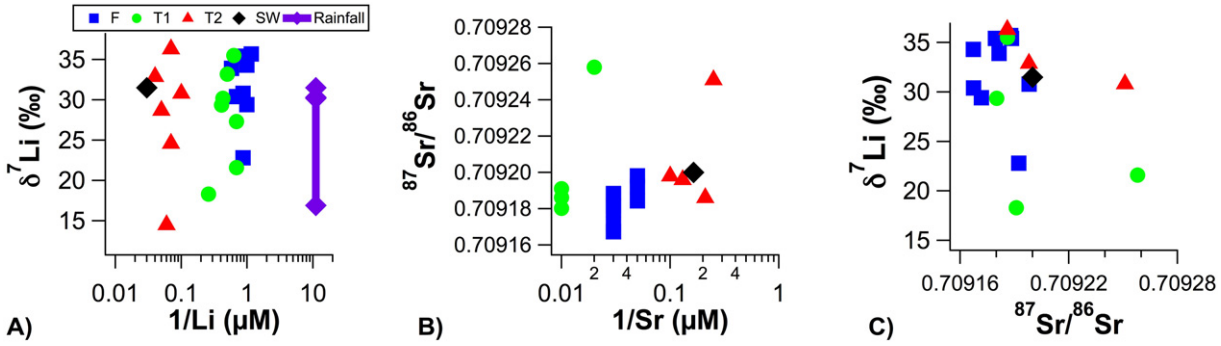

Fig. 4. A) δ^7Li values of rainfall and groundwater samples as a function of inverse Li concentrations with the; B) groundwater $^{87}Sr/^{86}Sr$ ratios as a function of inverse Sr concentrations with the average values shown for seawater. C) Groundwater $^{87}Sr/^{86}Sr$ ratios as a function of δ^7Li values. Seawater average values shown for δ^7Li (Misra and Froelich, 2012), and $^{87}Sr/^{86}Sr$ (Elderfield, 1986).

Sr also reflects multiple sources and/or processes. Furthermore, there was no correlation between the $^{87}Sr/^{86}Sr$ ratios and δ^7Li values of groundwaters at RI (Fig. 4C).

When considering all groundwaters, there was no clear trend between groundwater δ^7Li values and Cl concentrations (Fig. 2H), depth (Fig. 3C), or Li concentrations (Fig. 4); we therefore consider each groundwater type (i.e. fresh, T1 and T2) separately. The average δ^7Li value of each groundwater type decreased in the order of fresh groundwaters, T1 and T2 groundwaters with values of $+32.0 \pm 4.2$ ($n = 9$), $+28.6 \pm 6.0$ ($n = 8$) and $+28.0 \pm 7.7$‰ (1SD, $n = 6$), respectively. These groups all have similar maximum δ^7Li values (ca. +35‰) and the lower averages of the groundwater groups are strongly influenced by two lower δ^7Li values in T1 groundwaters and one very low δ^7Li value in T2 groundwaters. Furthermore, there was a correlation ($\rho = 0.70$, $p = 0.23$) between δ^7Li values and screen elevation for T2 groundwaters, but this is not statistically significant due to the small sample size (Fig. 3C). A local seawater sample obtained from the shoreline had a slightly higher δ^7Li value (+33.0‰) than the global seawater average of 31.5‰ (Misra and Froelich, 2012); since the δ^7Li value of local seawater is similar to the average value for the fresh groundwaters, it may indicate the occurrence of submarine groundwater discharge from the shoreline.

5.2.1. Rock and soil samples

The rock and soil samples (RI_B01B and RI_S01) from RI had somewhat similar Li and Sr abundances of ~0.2 and ~7 μM, respectively, and Li/Ca and Sr/Ca ratios of ~0.1 and ~3 μM/mM, respectively (Table 3). The acid-soluble fraction (0.5 M HCl) of the soil and rock had lower average Li/Ca and Sr/Ca ratios of 0.06 and 2.47 μM/mM, respectively. The low Al/Ca, Zr/Ca, Na/Ca (all <0.62 μM/mM) of the carbonate leaches indicate that the clays and other silicate minerals were not extensively leached during the experiment. The residual silicate portion of the rocks dissolved by strong acid dissolution had higher average Li/Ca and Sr/Ca ratios of 0.12 and 3.81 μM/mM, respectively.

The soil, paleosol and aeolianite samples (RI_S01, RI_B01B and RI_B03) predominantly comprised carbonate minerals (>90 wt%), with trace amounts (1–6 wt%) of quartz (Table 4). The highest abundance of quartz (6 wt%) was found in the soil sample RI_S01, compared to ~1 wt% in the paleosol and aeolianite Tamala Limestone units (RI_B01B and RI_B03). The proportion of quartz and feldspars in Tamala Limestone from RI is less than reported for aeolianite units from the Australian mainland, which ranged from 4 to 79 wt% (mean = 42 wt%) and 1 to 3 wt% (mean = 2 wt%), respectively (Lipar and Webb, 2014). The predominant forms of carbonate minerals in the soil, paleosol, and aeolianite samples were low-Mg calcite, high-Mg calcite, and aragonite; pure calcite was only detected in the aeolianite unit (26.3 wt%). Similar proportions of carbonate mineral compositions were reported for the Tamala Limestone aeolianite unit on the Australian mainland, except no pure calcite was detected (Lipar and Webb, 2014).

6. Discussion

We first constrain the proportions of Li and Sr sourced from atmospheric input, carbonate weathering and silicate weathering to estimate the initial $^{87}Sr/^{86}Sr$ ratio and δ^7Li value of fresh groundwaters following recharge. Following this, we discuss the evolution of groundwater δ^7Li values with respect to water-rock interactions in fresh groundwaters. Finally, we consider the effects of water-rock interactions in the older, deeper, and more saline T1 and T2 groundwaters.

6.1. Sources of Li and Sr in fresh groundwaters

Dissolved cations in fresh groundwaters are typically sourced from rainfall and by the near-surface dissolution of evaporite, silicate, and carbonate minerals; in coastal settings, large amounts of dissolved cations can also be provided by the deposition sea spray aerosols (Chadwick et al., 1999). Seawater mixing is unimportant for the fresh

Table 3
Elemental data for a soil (S01) and Tamala Limestone unit (B01) sampled from Rottnest Island[a].

Sample		Li	Sr	Ca	Al/Ca	Fe/Ca	K/Ca	Li/Ca	Mg/Ca	Na/Ca	Si/Ca	Sr/Ca	Zr/Ca	Sr/Li
		μM	μM	mM	μM/mM	μM/mM	μM/mM	μM/mM	μM/mM	μM/mM	μM/mM	μM/mM	μM/mM	μM/μM
B01	Acid soluble	0.01	0.54	0.22	0.46	0.23	1.89	0.07	71.90	0.20	0.11	2.45	0.10	36.03
S01	Acid soluble	0.01	0.55	0.22	0.62	0.15	0.29	0.06	79.27	0.20	0.05	2.48	0.05	41.70
B01	Residue	0.52	16.35	3.90	5.01	5.19	2.58	0.13	115.70	1.44	4.95	4.20	2.90	31.40
S01	Residue	0.33	10.13	2.78	12.84	3.11	9.04	0.12	124.01	2.02	10.75	3.65	7.64	30.28
B01	Bulk	0.48	12.77	3.38	3.44	3.69	2.80	0.14	109.15	1.66	0.68	3.78	6.28	26.42
S01	Bulk	0.35	13.61	3.54	5.10	1.29	4.03	0.10	122.92	1.58	3.37	3.84	3.99	38.52
Av.	Acid soluble	0.01	0.54	0.22	0.54	0.19	1.09	0.06	75.58	0.20	0.08	2.47	0.07	38.8
Av.	Residue	0.42	13.19	3.46	4.27	2.49	3.42	0.12	116.03	1.62	2.03	3.81	5.14	32.47
Av.	Bulk	0.18	7.08	1.88	2.86	0.72	2.16	0.08	101.1	0.89	1.71	3.16	2.02	40.11

[a] 1SD uncertainty for all elements is ±6.2%.

Table 4
XRD data for a soil and Tamala Limestone units sampled from Rottnest Island.

Sample	Description	Low-Mg calcite ($[Mg_{0.03}\ Ca_{0.97}]CO_3$)	High-Mg calcite ($[Mg_{0.129}\ Ca_{0.871}]CO_3$)	Calcite ($CaCO_3$)	Aragonite ($CaCO_3$)	Quartz (SiO_2)	Sylvine, sodian ($[K_{0.9}Na_{0.1}]Cl$)
		wt%	wt%	wt%	wt%	wt%	wt%
RI-S01	Soil	28.1	52.7	0	13.2	6.0	0.0
RI-B01B	Paleosol	34.9	46.7	0	15.2	1.1	0.0
RI-B03	Rock	40.7	16.8	26.3	14.7	1.2	0.3

groundwaters at RI, because they lie well above the freshwater-seawater mixing zone that is also indicated by their low (<1%) estimated seawater fractions (Bryan et al., 2016). Moreover, no evaporite minerals were detected in the Tamala Limestone (Table 4) and these are not considered as a source of cations at RI. However, sea salt aerosols and particles may significantly contribute to the compositions of surface waters and rainfall. The proportion of an element (X = Na, Ca, Li or Sr) in fresh groundwaters delivered from the atmosphere can be estimated using molar X/Cl ratios of rainfall and the groundwater Cl concentrations (Négrel et al., 1993) (see Table A.3 for molar concentrations of major cations and Cl). Rainfall samples from RI have an average molar Na/Cl ratio of 0.79 and have undergone little Cl degassing (Pio and Lopes, 1998), suggesting that rainfall on RI is locally derived with a dilute seawater-like composition. Therefore, the molar X/Cl ratios measured in rainfall may also represent the contribution of dissolved cations from sea-spray aerosols formed by wave and wind action (Chadwick et al., 1999). The combined contribution of dissolved Cl and from rainfall and sea-spray aerosols is referred to as 'atmospheric input'. In contrast, modern dust deposited from the atmosphere in the soil zone is considered to be represented in the silicate-derived fraction from the bedrock. The average Ca/Cl, Sr/Cl, and Li/Cl ratios in rainfall samples were 0.052 mM/mM, 0.23 μM/mM and 0.048 μM/mM, respectively. By considering these values, and the Cl concentrations in fresh groundwaters, we estimate that the atmospheric input contributes 16 ± 2 to 28 ± 4% and 3 ± 0.4 to 10 ± 2% of the dissolved Li and Sr in fresh groundwaters, respectively (see Table A.4 for a summary of individual and propagated uncertainties; Fig. 5). For major cations, we estimate that 10 ± 2 to 34 ± 5% and 85 ± 13 to 100 ± 15% of Ca and Na are sourced from atmospheric input that should be considered when estimating the amount of Li and Sr derived from carbonate and silicate weathering. Furthermore, the high proportions of dissolved Na sourced from atmospheric input means that Na is not appropriate for tracing silicate weathering interactions in a coastal aquifer, which may be applicable in non-coastal settings (Gaillardet et al., 1999).

Carbonate mineral dissolution is a key geochemical process in the unsaturated zone on RI during recharge, resulting in all fresh

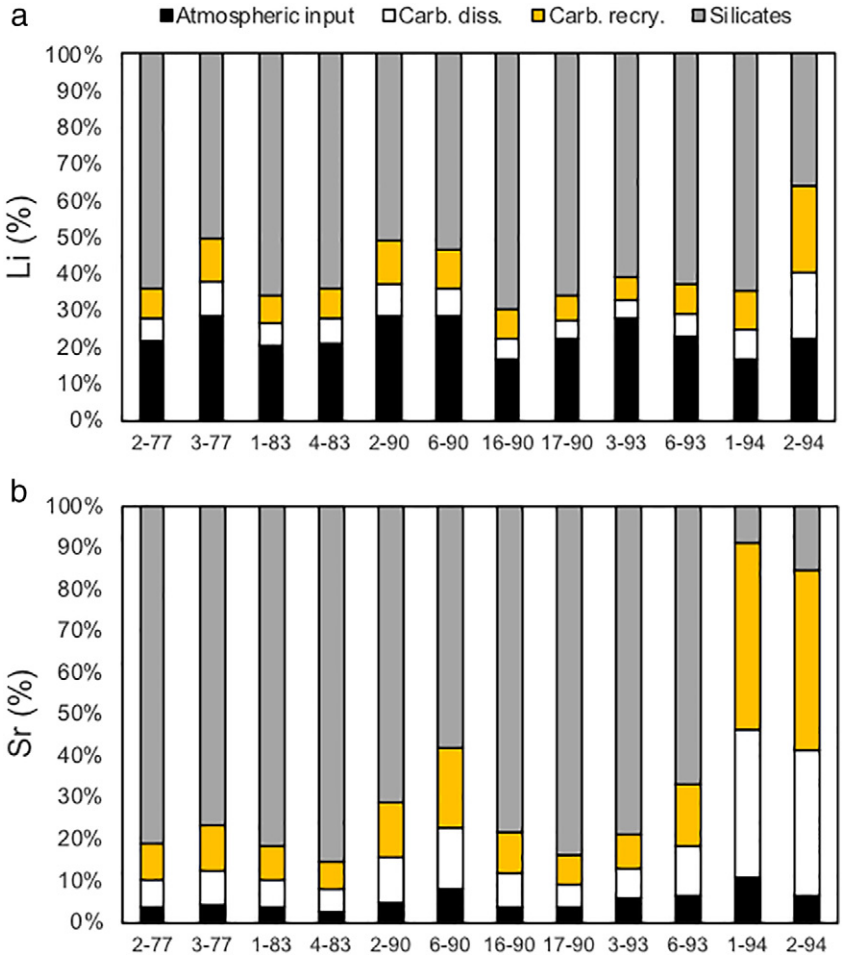

Fig. 5. Proportions of a) Li and b) Sr contributed by atmospheric input, silicate dissolution, carbonate dissolution ("carb. diss.") and carbonate recrystallisation ("carb. recry.") determined from mass balance considerations.

groundwaters being saturated with respect to calcite and aragonite (Bryan et al., 2017). The importance of dissolved carbonate as a source of Li and Sr can be considered by using the Li/Ca and Sr/Ca ratios of carbonates and the Ca concentrations in fresh groundwaters. The concentrations of Li and Sr were first corrected for atmospheric input using the molar X/Cl ratios of rainfall and the groundwater Cl concentrations.

The molar Li/Ca and Sr/Ca ratios of the carbonate end-member of the Tamala Limestone from the acid leaching experiments were 0.06 and 2.47 μmol/mmol, respectively. These values are remarkably similar to the average molar Li/Ca and Sr/Ca ratios of a marine biogenic carbonate compilation (n = 74, Dellinger et al., 2018), which were 0.08 and 2.50 μmol/mmol, respectively. This similarity is explained by the Tamala Limestone predominantly comprising marine biogenic carbonates with a high proportion of high-Mg calcite (Table 4) (Lipar and Webb, 2015). By combining these values with the Ca concentration of fresh groundwaters, the estimated amount of Li and Sr contributed by carbonate dissolution ranged from 5 ± 1 to 18 ± 3 and 5 ± 1 to 36 ± 5%, respectively (Fig. 5).

Another process that might contribute Li and Sr to the Rottnest groundwaters is carbonate recrystallisation as it may provide dissolved Li and Sr without increasing Ca. This process was considered using the Rayleigh fractional crystallisation calculation:

$$\frac{C_L}{C_0} = F^{(D-1)} \quad (1)$$

where C_0: concentration in parental liquid, C_L: concentration in differentiated liquid, F: fraction of liquid remaining, and D: bulk distribution coefficient for calcite precipitation. The value for F was constrained to be 0.77 by NETPATH modelling (Plummer et al., 1991) of the geochemical reactions between the freshest groundwater (well 2–94) and the most geochemically-evolved (based on TDS concentrations) fresh groundwater (well 3–77), indicating that 4.5 mmol/(kg H_2O) of high Mg-calcite would be dissolved and 3.5 mmol/(kg H_2O) of pure calcite would be precipitated (Bryan et al., 2017). The Li distribution coefficient ($D_{Li/Ca}$) into calcite required to constrain this effect is temperature dependent, which can be expressed using the Li/Ca ratios in carbonate minerals and the precipitating solution:

$$D_{Li/Ca} = (Li/Ca_{carbonate})/(Li/Ca_{solution}) \quad (2)$$

Lithium is not strongly incorporated into calcite in low-temperature groundwater settings with $D_{Li/Ca}$ decreasing from 0.009 at 5 °C to 0.003 at 30 °C (Marriott et al., 2004). The average temperature of groundwaters RI at the time of sampling was 18 °C, corresponding to a $D_{Li/Ca}$ value of 0.006. Similarly for Sr, the apparent $D_{Sr/Ca}$ ranges from 0.12 to 0.35 (Gabitov and Watson, 2006), and a value of 0.15 was chosen for $D_{Sr/Ca}$. By using Eq. (1), the amount of Li and Sr estimated to be released during calcite recrystallisation is estimated to range from 8–24% and 7–45%.

Silicate mineral dissolution typically exerts a strong control on the Li isotope composition of the dissolved load in carbonate lithologies (Kısakűrek et al., 2005; Pogge von Strandmann et al., 2017). In contrast, $^{87}Sr/^{86}Sr$ is influenced to a much greater extent by the dissolution of carbonate minerals in silicate lithologies (Blum et al., 1998), and evaporite minerals such as anhydrite (Jacobson and Wasserburg, 2005). Silicate minerals are present within the carbonate aeolianite matrix of the Tamala Limestone with a silicate mineral content of <6 wt% on RI (Table 4) and an average 42 wt% on the Australian mainland (Lipar and Webb, 2014). In addition, silicates are present in modern dust that are deposited in the soil-forming zone above the freshwater lens as mainly quartz (Table 4) and, as such, this aeolian contribution is not considered to be distinct from the bedrock-derived silicates present within the Tamala Limestone matrix. Although XRD measurements suggest that the silicate minerals are mainly quartz, a rough mass balance of Li and Sr contents of the Tamala Limestone suggests that ~50% of each element are sourced from the acid-soluble fraction and the residue (Table 3). This suggests that cations are supplied by the dissolution of fine-grained, poorly crystalline material within the bedrock, e.g. ferrihydrite (Navrotsky et al., 2008), which was not detected by XRD.

The proportions of Li and Sr in the fresh groundwaters that were contributed by silicate weathering in the aquifer were assumed to be the fractions of those elements remaining after accounting for atmospheric input, carbonate dissolution and calcite recrystallisation. Following this approach, the amounts of Li and Sr provided by silicate weathering are estimated to be 36 ± 8 to 70 ± 15% and 9 ± 2 to 86 ± 19% (see Appendix), respectively. Thus, the proportions of Li and Sr supplied by silicate dissolution appears to be highly variable, and, in some cases (RI_2-94 for Li and RI_1-94 and RI_2-94 for Sr), accounts for <50% of the dissolved Li, whereby the majority of Li instead comes from atmospheric input, carbonate dissolution and calcite recrystallisation (Fig. 5).

6.2. Initial Li and Sr isotope compositions of fresh groundwaters

The initial δ^7Li value of fresh groundwaters following recharge is an important parameter for understanding weathering reactions in the aquifer. This value can be assessed using a simple mass balance approach based on the estimated proportions of Li sourced from atmospheric input, carbonates and silicates, which have average values of 23, 8 and 69%, respectively. Atmospheric input is likely to be influenced predominantly by rainfall during winter when rainfall is more intense and evaporation rates are lower (Bryan et al., 2016). The δ^7Li values of winter rainfall would then imply that the average δ^7Li values of recharge waters will be similar to seawater (~31‰) (Table 1). Lithium sourced from carbonate minerals should largely be influenced by the dissolution of high-Mg calcite and aragonite minerals present within the Tamala Limestone as these minerals dissolve faster low-Mg and pure calcite (Appelo and Postma, 2005), and have higher Li/Ca values (Dellinger et al., 2018). As high-Mg calcite and aragonite have δ^7Li values ranging from 25 to 40‰ (Dellinger et al., 2018), we assume an average value of 32.5‰. Finally, the average isotopic composition of Li sourced from silicate minerals is assumed to represent the average value of the upper continental crust (4‰) (Teng et al., 2004). By adopting these compositions for the various reservoirs, we estimate that the initial δ^7Li value of meteoric recharge waters is 16‰. Although the δ^7Li values of the carbonate and atmospheric input components are poorly constrained, the estimated initial δ^7Li value of recharge waters is not sensitive to changes in the Li isotope composition of these sources due to the lower estimated proportion of Li and Sr sourced from these reservoirs. For instance, assigning δ^7Li values of 40‰ to both the atmospheric input and carbonate dissolution would only increase the expected initial δ^7Li value of recharge waters from 16 to 18‰. As the δ^7Li value of fresh groundwaters are all >22.8‰ (Table 2), we suggest that water-rock interactions occur during recharge and increase the δ^7Li value by >6‰.

Unlike Li isotopes, the $^{87}Sr/^{86}Sr$ ratio of groundwaters is not affected by isotopic fractionation during secondary mineral formation and adsorption onto clay minerals, but is mainly controlled by the dissolution kinetics of the different carbonate minerals in the aquifer with a contribution from silicate minerals, which typically have elevated Rb/Sr and $^{87}Sr/^{86}Sr$ ratios. Although XRD measurements suggest that the non-carbonate minerals within the Tamala Limestone are predominantly quartz (Table 4), the relatively modest Si/Ca of the acid-insoluble residues suggest a substantial contribution from material other than quartz in the residue (Table 3). This material could be undissolved carbonate minerals or fine-grained, poorly crystalline minerals, e.g. ferrihydrite (Navrotsky et al., 2008), that were not detected in XRD measurements, but may have been deposited as dust during the Late Quaternary and would have negligible Sr contents and low Rb/Sr ratios. In addition, modern dust deposited in the soil-forming zone above the freshwater lens may also provide silicate-derived Li and Sr, which would also be carried mainly by quartz grains (Table 4). The

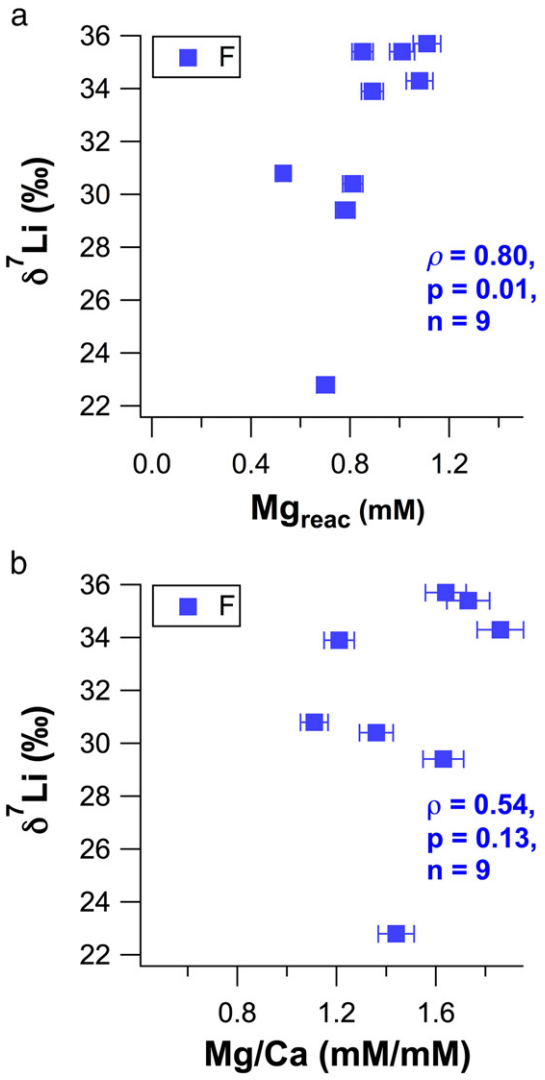

Fig. 6. δ^7Li values of F groundwaters as a function of a) Mg excess calculated by PHREEQC (Mg_{reac}) and b) molar Mg/Ca ratios where ρ: Spearman's rank correlation coefficient.

high Sr and Li concentrations, and Al/Ca, Fe/Ca, and K/Ca ratios in the acid-insoluble residue relative to the acid soluble fraction support the hypothesis that there is a substantial contribution of these cations in groundwaters from the dissolution fine-grained, poorly crystalline minerals that were not detected by XRD, e.g. ferrihydrite (Navrotsky et al., 2008), or other phases with the elemental characteristics implied by the residue compositions. A similar influence of poorly crystalline material has been observed elsewhere with clay-rich, former aeolian soils forming above limestone, e.g. cave drip waters at Wellington Caves have the mixed imprint of clay-mineral interactions and limestone dissolution (Rutlidge et al., 2014). The $^{87}Sr/^{86}Sr$ ratios of fresh groundwaters at RI ranged from 0.70917 to 0.70920 (Table 2), marginally less than the mean $^{87}Sr/^{86}Sr$ ratio of modern seawater (0.70924) (Elderfield, 1986). Based on mass balance calculations we estimate that at least ~50% of Sr is provided by the weathering of silicate minerals (see Section 6.1). As a more radiogenic Sr source (higher $^{87}Sr/^{86}Sr$) would increase the $^{87}Sr/^{86}Sr$ ratio of fresh groundwaters relative to the seawater value, we infer that the aeolian-derived quartz in the Tamala Limestone and the modern soil-forming zone has an $^{87}Sr/^{86}Sr$ ratio around 0.7092. Unfortunately, the $^{87}Sr/^{86}Sr$ ratios are not especially useful for constraining the Sr budget in fresh groundwaters as modern seawater, Late Quaternary carbonates and coastal rainfall in Australia also have $^{87}Sr/^{86}Sr$ ratios around ~0.7092 (Elderfield, 1986; Raiber et al., 2009).

6.3. Lithium isotope fractionation in fresh groundwaters

6.3.1. Carbonate reactions

There is a correlation between excess Mg and high δ^7Li values in fresh groundwaters ($\rho = 0.80$, p = 0.01, n = 9, Fig. 6a) and to a lesser extent between δ^7Li values and molar Mg/Ca ratios but the latter is not statistically significant ($\rho = 0.54$, p = 0.13, n = 9, Fig. 6b). These relationships may be explained by the incongruent dissolution of high-Mg calcite or aragonite phases, which are abundant in the Tamala Limestone (Table 4), and the formation of more stable low-Mg calcite (Appelo and Postma, 2005):

$$(Ca_{1-x}Mg_x)CO_3 + H_2CO_3 \rightleftharpoons (1-x)Ca^{2+} + xMg^{2+} + 2HCO3_2^- \quad (3)$$

However, the $D_{Li/Ca}$ value in RI groundwaters is low (~0.006) (Marriott et al., 2004); thus, the proportion of dissolved Li removed from solution and incorporated into low-Mg calcite would not be large enough to produce isotopic fractionation. A more likely explanation for the suggested relationship between excess Mg and δ^7Li values in fresh groundwaters is preferential dissolution of high-Mg calcite relative to low-Mg calcite (Appelo and Postma, 2005), due to the correspondingly higher δ^7Li values (25 to 40‰) of high-Mg calcites (Dellinger et al., 2018). Our mass balance considerations estimate that 8–24% of dissolved Li in fresh groundwaters is sourced from carbonate minerals during recrystallisation. Thus, the preferential dissolution of high-Mg carbonates with high δ^7Li values appears to somewhat increase the δ^7Li values of fresh groundwaters. It is also likely that covariables, such as groundwater age and extent of secondary mineral reactions, also vary with the groundwater Mg excess and molar Mg/Ca ratio, thereby increasing the δ^7Li values of fresh groundwaters.

6.3.2. Mineral surface interactions

The enrichment of ^{7}Li in natural waters relative to primary silicate minerals is often attributed to the preferential uptake of ^{6}Li during clay mineral formation (Vigier et al., 2008). Despite the high δ^7Li values in fresh groundwaters, PHREEQC modelling using the standard "phreeqc.dat" database (Parkhurst and Appelo, 2013) suggests that all of the fresh groundwaters studied here were undersaturated in aluminosilicate clay minerals, but saturated in SiO_2 (Table 5). Therefore, the SiO_2 precipitate may preferentially incorporate ^{6}Li, producing the high δ^7Li values groundwater values. In addition to silica precipitation, preferential uptake of ^{6}Li can also occur during Li adsorption onto pre-existing clays and other minerals with high cation-exchange capacities, such as iron oxides and oxyhydroxides (Pistiner and Henderson, 2003) that are likely present in paleosol units within the Tamala Limestone that contain iron-rich and clay minerals, and high organic matter contents (Playford et al., 1977; Lipar and Webb, 2015). Therefore, we suggest that silica precipitation and Li adsorption onto aquifer units are likely responsible for Li isotope fractionation in fresh groundwaters following recharge. This process is consistent with results from other shallow coastal groundwater settings, such as Laizhou Bay, China, where it was found that slow silicate mineral weathering and hydraulic

Table 5
Mineral saturation states for fresh groundwaters modelled using PHREEQC3[a].

Phase	X	SI_3-77 (fresh)	SI_2-94 (mature)
Aragonite	$CaCO_3$	−0.12	0.10
Calcite	$CaCO_3$	0.03	0.24
Dolomite	$CaMg(CO_3)_2$	0.29	0.21
Gibbsite	$Al(OH)_3$	−1.56	−1.81
Gypsum	$CaSO_4{:}2H_2O$	−2.04	−2.08
K-feldspar	$KAlSi_3O_8$	−3.88	−3.85
K-mica	$KAl_3Si_3O_{10}(OH)_2$	−1.44	−1.90
Kaolinite	$Al_2Si_2O_5(OH)_4$	−2.2	−2.47
Quartz	SiO_2	0.07	0.18

[a] Parkhurst and Appelo (2013).

interactions between surface water and shallow groundwater controls Li isotope fractionation rather than seawater incursion (Qi et al., 2019). At RI, we find that the extent of Li isotope fractionation in fresh groundwater samples is likely a function of the specific groundwater flow path and the extent to which they interact with paleosol units in the Tamala Limestone.

6.4. Water-rock interactions in the freshwater-seawater transition zone

Two water types were identified previously in the freshwater-seawater transition zone based on the chemical and isotopic composition of the groundwater: T1 and T2 (Bryan et al., 2017). The T2 groundwaters are the deepest, most saline and oldest groundwaters, and T1 groundwaters have a composition that is intermediate between the F groundwaters and the more saline T2 groundwaters, probably due to tidal and groundwater level fluctuations within the transition zone. There is a general decrease in average δ^7Li values from fresh groundwaters (+32.0‰) to T1 (+28.6‰) and T2 groundwaters (+28.0‰). Furthermore, the δ^7Li values of the T2 groundwaters decrease with depth towards a δ^7Li value of +14.5‰ (Fig. 3B). We suggest that this is evidence of increased dissolution of low-δ^7Li material in the deeper aquifer from the silicate-rich basement rocks that underlie the Tamala Limestone, such as the Leederville or Yarragadee Sandstone aquifers (Playford et al., 1977). This would lower the δ^7Li value of T2 groundwaters as silicate minerals in the upper continental crust have an average of 0‰ (Teng et al., 2004) and clay minerals have low δ^7Li values due to the preferential uptake of ^{6}Li (Pistiner and Henderson, 2003; Vigier et al., 2008). The increased silicate dissolution rate in the deeper aquifer may be explained by a shift in the redox state of T2 groundwaters, which exhibit a sulfate deficit (Bryan et al., 2017). The generalised reaction scheme for microbially-mediated sulfate reduction (MSR) is:

$$SO_4^{2-} + 2CH_2O \rightarrow HS^- + H^+ + 2HCO_3^- \quad (4)$$

In this scenario, sulfate reduction produces 1 mol of H^+ for every mole of SO_4^{2-} reduced and may locally decrease the pH, thereby increasing the silicate dissolution rate as has been observed in many other coastal carbonate aquifers globally, e.g. The Bahamas (Bottrell et al., 1991). This supports the hypothesis that the deeper T2 groundwaters are somewhat isolated from contemporaneous seawater, which is supported by the absence of ^{3}H and low $^{14}C_{DIC}$ and $^{14}C_{DOC}$ contents and would be consistent with an approximate groundwater residence time of 3–7 ka in the deeper aquifer (Bryan et al., 2017).

7. Conclusions

In this study, we presented a Li and Sr isotope dataset of rainfall and groundwater samples from a carbonate island aquifer system, Rottnest Island, Western Australia to further understand water-rock interactions in such environments. Mass balance considerations suggest that silicates are the major source of Li and Sr in fresh groundwaters that are quartz and fine-grained, poorly-crystalline minerals, such as ferrihydrite, hosted within the Tamala Limestone the bedrock. For Li, atmospheric input via rainfall and sea-spray aerosols is the second most important source followed by carbonate dissolution. In contrast, carbonate dissolution is more important for Sr compared to atmospheric input. The Sr isotope compositions of groundwaters are relatively constant throughout the aquifer and exhibit a seawater-like average composition of 0.709192. The δ^7Li value of the groundwater following recharge is estimated to be ca. +10 to 15‰ and we propose that Li isotopes are rapidly fractionated by water-rock interactions during recharge as the δ^7Li values in fresh groundwaters ranged from +22 to +35‰. Due to undersaturation of clay minerals in fresh groundwaters, we attribute the increase in the δ^7Li values in these groundwaters primarily to Li adsorption onto surfaces with high cation-exchange capacities, e.g. iron (oxy)hydroxides and clay minerals present within Late Quaternary paleosol units that occur in the Tamala Limestone. Moreover, the range of δ^7Li values and the high spatial resolution of the sampled groundwater wells reveals that Li concentrations and δ^7Li values are spatially variable over a small area (<20 km^2) that may be due to the specific groundwater flow path and interactions with paleosol units. In deeper groundwaters, we observed a decrease in the average δ^7Li value of groundwaters with increasing depth and extent of seawater mixing. The lowest δ^7Li value (+14.5‰) for all groundwaters was found at the greatest depth in the aquifer. As the aquifer is underlain by silicate-rich basement rocks and silicate and/or clay minerals have lower δ^7Li values, we suggest that this deeper groundwater has interacted with the basement rocks in the freshwater-seawater transition zone. Overall, this study shows that coastal carbonate aquifers are not simple seawater mixing zones and a high degree of Li isotope fractionation can occur as a result of water-rock interactions within the aquifer.

Declaration of competing interest

The authors declare that they have no known competing financial interests or personal relationships that could have appeared to influence the work reported in this paper.

Acknowledgements

We thank the Rottnest Island Authority (RIA), especially Cassyanna Thomas, Luke Wheat and Shane Kearney for supporting this project. We also thank Dr. Suzanne Hollins, Head of Research at the Australian Nuclear Science and Technology Organisation (ANSTO) for her ongoing support as well as various ANSTO personnel including, Henri Wong and Chris Vardanega for their assistance in ICP-MS and ICP-OES analysis, and Chris Dimovski and Stuart Hankin for their assistance with field trip preparation, and Krista Simon and David Child for use of the clean laboratory facilities. We thank Dr. Chris Marjo from the Mark Wainwright Analytical Centre at UNSW for their assistance with XRD analyses. We kindly thank Les Kinsley for sharing his expertise during MC-ICPMS analyses at ANU. Two anonymous journal reviews and the Associate Editor (Prof. Mae S. Gustin) are thanked for improving the clarity and quality of this manuscript.

This work was supported Australian Research Council Linkage grant LP150100144.

Appendix A. Supplementary data

Supplementary data to this article can be found online at https://doi.org/10.1016/j.scitotenv.2020.136906.

References

Albarède, F., Beard, B., 2004. Analytical methods for non-traditional isotopes. Rev. Mineral. Geochem. 55, 113–152.
Appelo, C., Postma, D., 2005. Geochemistry, Groundwater and Pollution. AA Balkema, Rotterdam, Netherlands.
Bagard, M.-L., West, A.J., Newman, K., Basu, A.R., 2015. Lithium isotope fractionation in the Ganges–Brahmaputra floodplain and implications for groundwater impact on seawater isotopic composition. Earth Planet. Sci. Lett. 432, 404–414.
Banner, J.L., Musgrove, M., Capo, R., 1994. Tracing ground-water evolution in a limestone aquifer using Sr isotopes: effects of multiple sources of dissolved ions and mineral-solution reactions. Geology 22, 687–690.
Beck, A.J., Charette, M.A., Cochran, J.K., Gonneea, M.E., Peucker-Ehrenbrink, B., 2013. Dissolved strontium in the subterranean estuary–implications for the marine strontium isotope budget. Geochim. Cosmochim. Acta 117, 33–52.
Blum, J.D., Gazis, C.A., Jacobson, A.D., Page Chamberlain, C., 1998. Carbonate versus silicate weathering in the Raikhot watershed within the High Himalayan Crystalline Series. Geology 26, 411–414.
Bottrell, S.H., Smart, P.L., Whitaker, F., Raiswell, R., 1991. Geochemistry and isotope systematics of sulphur in the mixing zone of Bahamian blue holes. Appl. Geochem. 6, 97–103.
Brooke, B., 2001. The distribution of carbonate eolianite. Earth Sci. Rev. 55, 135–164.

Bryan, E., Meredith, K.T., Baker, A., Post, V.E., Andersen, M.S., 2016. Island groundwater resources, impacts of abstraction and a drying climate: Rottnest Island, Western Australia. J. Hydrol. 542, 704–718.

Bryan, E., Meredith, K.T., Baker, A., Andersen, M.S., Post, V.E.A., 2017. Carbon dynamics in a Late Quaternary-age coastal limestone aquifer system undergoing saltwater intrusion. Sci. Total Environ. 607–608, 771–785.

Bryan, E., Meredith, K.T., Baker, A., Andersen, M.S., Post, V.E., Treble, P.C., 2020. How water isotopes (18O, 2H, 3H) within an island freshwater lens respond to changes in rainfall. Water Res. 170, 115301.

Chadwick, O.A., Derry, L.A., Vitousek, P.M., Huebert, B.J., Hedin, L.O., 1999. Changing sources of nutrients during four million years of ecosystem development. Nature 397, 491.

Clergue, C., Dellinger, M., Buss, H.L., Gaillardet, J., Benedetti, M.F., Dessert, C., 2015. Influence of atmospheric deposits and secondary minerals on Li isotopes budget in a highly weathered catchment, Guadeloupe (Lesser Antilles). Chem. Geol. 414, 28–41.

Dellinger, M., West, A.J., Paris, G., Adkins, J.F., von Strandmann, P.A.P., Ullmann, C.V., Eagle, R.A., Freitas, P., Bagard, M.-L., Ries, J.B., 2018. The Li isotope composition of marine biogenic carbonates: patterns and mechanisms. Geochim. Cosmochim. Acta 236, 315–335.

DePaolo, D.J., 2011. Surface kinetic model for isotopic and trace element fractionation during precipitation of calcite from aqueous solutions. Geochim. Cosmochim. Acta 75, 1039–1056.

Dürr, H.H., Meybeck, M., Dürr, S.H., 2005. Lithologic composition of the Earth's continental surfaces derived from a new digital map emphasizing riverine material transfer. Glob. Biogeochem. Cycles 19, 1–22.

Elderfield, H., 1986. Strontium isotope stratigraphy. Palaeogeogr. Palaeoclimatol. Palaeoecol. 57, 71–90.

Gabitov, R.I., Watson, E.B., 2006. Partitioning of strontium between calcite and fluid. Geochem. Geophys. Geosyst. 7, 1–12.

Gaillardet, J., Dupré, B., Louvat, P., Allégre, C., 1999. Global silicate weathering and CO_2 consumption rates deduced from the chemistry of large rivers. Chem. Geol. 159, 3–30.

Garrels, R.M., Mackenzie, F.T., 1967. Origin of the chemical compositions of some springs and lakes. In: Gould, R.F. (Ed.), Equilibrium Concepts in Natural Water Systems ACS Publications. Am. Chem. Sot. Adv. Chem. Ser, pp. 222–242.

Goldenberg, L., Magaritz, M., Amiel, A., Mandel, S., 1984. Changes in hydraulic conductivity of laboratory sand-clay mixtures caused by a seawater-freshwater interface. J. Hydrol. 70, 329–336.

Gouramanis, C., Dodson, J., Wilkins, D., De Deckker, P., Chase, B., 2012. Holocene palaeoclimate and sea level fluctuation recorded from the coastal Barker Swamp, Rottnest Island, south-western Western Australia. Quat. Sci. Rev. 54, 40–57.

Hartmann, J., Moosdorf, N., 2012. The new global lithological map database GLiM: a representation of rock properties at the Earth surface. Geochem. Geophys. Geosyst. 13, 1–37.

Huh, Y., Chan, L.-H., Zhang, L., Edmond, J.M., 1998. Lithium and its isotopes in major world rivers: implications for weathering and the oceanic budget. Geochim. Cosmochim. Acta 62, 2039–2051.

Jacobson, A., Wasserburg, G., 2005. Anhydrite and the Sr isotope evolution of groundwater in a carbonate aquifer. Chem. Geol. 214, 331–350.

Kısakűrek, B., James, R.H., Harris, N.B., 2005. Li and δ7Li in Himalayan rivers: proxies for silicate weathering? Earth Planet. Sci. Lett. 237, 387–401.

Lipar, M., Webb, J., 2014. Middle–late Pleistocene and Holocene chronostratigraphy and climate history of the Tamala Limestone, Cooloongup and Safety Bay Sands, Nambung National Park, southwestern Western Australia. Aust. J. Earth Sci. 61, 1023–1039.

Lipar, M., Webb, J.A., 2015. The formation of the pinnacle karst in Pleistocene aeolian calcarenites (Tamala Limestone) in southwestern Australia. Earth Sci. Rev. 140, 182–202.

Liu, X.-M., Wanner, C., Rudnick, R.L., McDonough, W.F., 2015. Processes controlling δ7Li in rivers illuminated by study of streams and groundwaters draining basalts. Earth Planet. Sci. Lett. 409, 212–224.

Magaritz, M., Luzier, J.E., 1985. Water-rock interactions and seawater-freshwater mixing effects in the coastal dunes aquifer, Coos Bay, Oregon. Geochim. Cosmochim. Acta 49, 2515–2525.

Maher, K., 2011. The role of fluid residence time and topographic scales in determining chemical fluxes from landscapes. Earth Planet. Sci. Lett. 312, 48–58.

Marriott, C.S., Henderson, G.M., Belshaw, N.S., Tudhope, A.W., 2004. Temperature dependence of δ7Li, δ44 Ca and Li/Ca during growth of calcium carbonate. Earth Planet. Sci. Lett. 222, 615–624.

Martin, J.B., Moore, P.J., 2008. Sr concentrations and isotope ratios as tracers of groundwater circulation in carbonate platforms: examples from San Salvador Island and Long Island, Bahamas. Chem. Geol. 249, 52–65.

Meredith, K., Moriguti, T., Tomascak, P., Hollins, S., Nakamura, E., 2013. The lithium, boron and strontium isotopic systematics of groundwaters from an arid aquifer system: implications for recharge and weathering processes. Geochim. Cosmochim. Acta 112, 20–31.

Millot, R., Guerrot, C., Vigier, N., 2004. Accurate and high-precision measurement of lithium isotopes in two reference materials by MC-ICP-MS. Geostand. Geoanal. Res. 28, 153–159.

Millot, R., Petelet-Giraud, E., Guerrot, C., Négrel, P., 2010. Multi-isotopic composition (δ7Li–δ11B–δD–δ18O) of rainwaters in France: Origin and spatio-temporal characterization. Appl. Geochem. 25 (10), 1510–1524.

Millot, R., Guerrot, C., Innocent, C., Négrel, P., Sanjuan, B., 2011. Chemical, multi-isotopic (Li–B–Sr–U–H–O) and thermal characterization of Triassic formation waters from the Paris Basin. Chem. Geol. 283, 226–241.

Misra, S., Froelich, P.N., 2012. Lithium isotope history of Cenozoic seawater: changes in silicate weathering and reverse weathering. Science 335, 818–823.

Murphy, M.J., Strandmann, P.A.E.P., Porcelli, D., Ingri, J., 2014. Li isotope behaviour in the low salinity zone during estuarine mixing. Prog Earth Planet Sci 10, 204–207.

Navrotsky, A., Mazeina, L., Majzlan, J., 2008. Size-driven structural and thermodynamic complexity in iron oxides. Science 319, 1635–1638.

Négrel, P., Allègre, C.J., Dupré, B., Lewin, E., 1993. Erosion sources determined by inversion of major and trace element ratios and strontium isotopic ratios in river water: the Congo Basin case. Earth Planet. Sci. Lett. 120, 59–76.

Négrel, P., Millot, R., Guerrot, C., Petelet-Giraud, E., Brenot, A., Malcuit, E., 2012. Heterogeneities and interconnections in groundwaters: coupled B, Li and stable-isotope variations in a large aquifer system (Eocene Sand aquifer, Southwestern France). Chem. Geol. 296–297, 83–95.

Parkhurst, D.L., Appelo, C., 2013. Description of Input and Examples for PHREEQC Version 3: A Computer Program for Speciation, Batch-reaction, One-dimensional Transport, and Inverse Geochemical Calculations. US Geological Survey.

Pio, C.A., Lopes, D.A., 1998. Chlorine loss from marine aerosol in a coastal atmosphere. J. Geophys. Res.-Atmos. 103, 25263–25272.

Pistiner, J.S., Henderson, G.M., 2003. Lithium-isotope fractionation during continental weathering processes. Earth Planet. Sci. Lett. 214, 327–339.

Playford, P.E., 1997. Geology and Hydrogeology of Rottnest Island, Western Australia.

Playford, P.E., Low, G., Cockbain, A.E., 1976. Geology of the Perth Basin, Western Australia. Geological Survey of Western Australia.

Playford, P.E., Leech, R., Kendrick, G.W., 1977. Geology and Hydrology of Rottnest Island. Geological Survey of Western Australia.

Plummer, L.N., Prestemon, E.C., Parkhurst, D.L., 1991. An interactive code (NETPATH) for modeling net geochemical reactions along a flow path. Water-Resources Investigations Report 91, 4078.

Pogge von Strandmann, P.A.E., Henderson, G.M., 2015. The Li isotope response to mountain uplift. Geology 43, 67–70.

Pogge von Strandmann, P.A.E., Burton, K.W., James, R.H., van Calsteren, P., Gíslason, S.R., Mokadem, F., 2006. Riverine behaviour of uranium and lithium isotopes in an actively glaciated basaltic terrain. Earth Planet. Sci. Lett. 251, 134–147.

Pogge von Strandmann, P.A., James, R.H., van Calsteren, P., Gíslason, S.R., Burton, K.W., 2008. Lithium, magnesium and uranium isotope behaviour in the estuarine environment of basaltic islands. Earth Planet. Sci. Lett. 274, 462–471.

Pogge von Strandmann, P.A., Burton, K.W., James, R.H., van Calsteren, P., Gislason, S.R., 2010. Assessing the role of climate on uranium and lithium isotope behaviour in rivers draining a basaltic terrain. Chem. Geol. 270, 227–239.

Pogge von Strandmann, P.A.E., Porcelli, D., James, R.H., van Calsteren, P., Schaefer, B., Cartwright, I., Reynolds, B.C., Burton, K.W., 2014. Chemical weathering processes in the Great Artesian Basin: evidence from lithium and silicon isotopes. Earth Planet. Sci. Lett. 406, 24–36.

Pogge von Strandmann, P.A.E., Vaks, A., Bar-Matthews, M., Ayalon, A., Jacob, E., Henderson, G.M., 2017. Lithium isotopes in speleothems: temperature-controlled variation in silicate weathering during glacial cycles. Earth Planet. Sci. Lett. 469, 64–74.

Qi, H., Taylor, P., Berglund, M., De Bievre, P., 1997. Calibrated measurements of the isotopic composition and atomic weight of the natural Li isotopic reference material IRMM-016. Int. J. Mass Spectrom. Ion Process. 171, 263–268.

Qi, H., Ma, C., He, Z., Hu, X., Gao, L., 2019. Lithium and its isotopes as tracers of groundwater salinization: a study in the southern coastal plain of Laizhou Bay, China. Sci. Total Environ. 650, 878–890.

Raiber, M., Webb, J.A., Bennetts, D.A., 2009. Strontium isotopes as tracers to delineate aquifer interactions and the influence of rainfall in the basalt plains of southeastern Australia. J. Hydrol. 367, 188–199.

Rutlidge, H., Baker, A., Marjo, C.E., Andersen, M.S., Graham, P.W., Cuthbert, M.O., Rau, G.C., Roshan, H., Markowska, M., Mariethoz, G., 2014. Dripwater organic matter and trace element geochemistry in a semi-arid karst environment: implications for speleothem paleoclimatology. Geochim. Cosmochim. Acta 135, 217–230.

Teng, F.Z., McDonough, W.F., Rudnick, R.L., Dalpé, C., Tomascak, P.B., Chappell, B.W., Gao, S., 2004. Lithium isotopic composition and concentration of the upper continental crust. Geochim. Cosmochim. Acta 68, 4167–4178.

Tomascak, P.B., Hemming, N.G., Hemming, S.R., 2003. The lithium isotopic composition of waters of the Mono Basin, California. Geochim. Cosmochim. Acta 67, 601–611.

Vacher, L.H., Quinn, T.M., 1997. Geology and Hydrogeology of Carbonate Islands. Elsevier.

Van Hoecke, K., Belza, J., Croymans, T., Misra, S., Claeys, P., Vanhaecke, F., 2015. Single-step chromatographic isolation of lithium from whole-rock carbonate and clay for isotopic analysis with multi-collector ICP-mass spectrometry. J. Anal. At. Spectrom. 30, 2533–2540.

Vigier, N., Godderis, Y., 2015. A new approach for modeling Cenozoic oceanic lithium isotope paleo-variations: the key role of climate. Clim. Past Discuss. 11, 635–645.

Vigier, N., Decarreau, A., Millot, R., Carignan, J., Petit, S., France-Lanord, C., 2008. Quantifying Li isotope fractionation during smectite formation and implications for the Li cycle. Geochim. Cosmochim. Acta 72, 780–792.

Zektser, I., Loaiciga, H.A., 1993. Groundwater fluxes in the global hydrologic cycle: past, present and future. J. Hydrol. 144, 405–427.